Comparison of particle swarm optimization and asynchronous particle swarm optimization for inverse scattering of a two-dimensional perfectly conducting cylinder

Chien-Ching Chiu*, Chi-Hsien Sun and Wan-Ling Chang
Electrical Engineering Department, Tamkang University, Tamsui, Taiwan

Abstract. This paper reports a two dimensional time domain inverse scattering algorithm based upon the finite-difference time domain method for determining the shape of perfectly conducting cylinder. Finite difference time domain method (FDTD) is used to solve the scattering electromagnetic wave of a perfectly conducting cylinder. The inverse problem is resolved by an optimization approach and the global searching scheme asynchronous particle swarm optimization (APSO) is then employed to search the parameter space. By properly processing the scattered field, some EM properties can be reconstructed. One is the location of the conducting cylinder, the others is the shape of the perfectly conducting cylinder. This method is tested by several numerical examples; numerical results indicate that the APSO outperforms the PSO in terms of reconstruction accuracy and convergence speed. Both techniques have been tested in the case of simulated measurements contaminated by additive white Gaussian noise.

1. Introduction

Numerical inverse scattering studies found in the literature are based on either frequency or time domain approaches. With frequency domain algorithms, the interaction of the entire medium with the incident field is considered simultaneously [1,5]. Time domain approaches can exploit causality to limit the region of inversion, potentially reducing the number of unknowns. Time domain inverse scattering problems somewhat related to the present study commonly appear in the area of geosciences and remote sensing [6,8]. The scatterer reconstruction belongs to the general category of limited angle microwave imaging problems. These problems are both nonlinear and ill-posed [9]. The nonlinearity emerges from the fact that the scattered field is a nonlinear function of the electromagnetic properties of the scatterers due to multiple scattering phenomena. On the other hand, the ill-posedness appears because the operator that maps the scatterer properties to the scattered field is compact [9].

In general, the nonlinearity of the problem is coped with by applying iterative optimization techniques [10,15], these algorithms based on stochastic strategies, offer advantages relative to local inversion algorithms including strong search ability simplicity, robustness, and insensitivity to ill-posedness.

*Corresponding author. Dr. Chien-Ching Chiu, Department of Electrical Engineering, Tamkang University, Tamsui 25137, Taiwan. Fax: +886 2 26209814; E-mail: chiu@ee.tku.edu.tw.

Compared with genetic algorithm (GA), particle swarm optimization (PSO) is much easier to implement and converge faster. Concerning the shape reconstruction of conducting scatterers, the PSO has been investigated whereas the PSO has been utilized in the reconstruction of dielectric scatterers [16]. In this case, the reported results indicate that the PSO is reliable tools for inverse scattering applications. Moreover, it has been shown that both differential evolution (DE) and PSO outperform real-coded GA in terms of convergence speed [17,18]. In recent decade years, some papers have compared different algorithm in inverse scattering [19,21]. However, to our knowledge, a comparative study about the performances of particle swarm optimization (PSO) and asynchronous particle swarm optimization (APSO) when applied to inverse scattering problems has not yet been investigated.

In recently ten years, Chiu [3,4] have applied the GA for the inversion of buried or immersed perfectly conducting cylinders with the geometry described by a Fourier series. Alternatively, Zhou [26] and Chiu [27,30] used cubic-spline to describe the geometry of a perfect conducting cylinder. The 2-D perfectly conducting cylinders are denoted by local shape functions $\rho = F(\theta)$ with respect to their local origins which can be continuous or discrete.

There are two main advantages for cubic-spline expansion as following: (i) For complicated shape, the number of unknown for expanding the shape function by cubic-spline expansion is less than that by Fourier series expansion. (ii) The exact center of the object is insensitive for cubic-spline expansion instead of Fourier series expansion. If there is some displacement for the exact center of the object, the number of unknown for expanding the shape function by Fourier series expansion will increase a lot. On the other hand, the number of unknown does not vary for cubic-spline expansion.

The present work focuses on comparing these two methods for inverse scattering problems under time domain. The forward problem is solved by the FDTD method, for which the subgridding technique [22] is implemented to closely describe the fine structure of the cylinder. The inverse problem is formulated into an optimization one, and then the global searching PSO and APSO are used to search the parameter space. Cubic spline interpolation technique [23] is employed to reduce the number of parameters needed to closely describe a cylinder of arbitrary shape as compared to the Fourier series expansion. In section II, the subgridding FDTD method for the forward scattering are presented. In section III and IV, inverse problem and the numerical results of the proposed inverse problem are given, respectively. Finally, in V section some conclusions are drawn for the proposed time domain inverse scattering.

2. Forward problem

Let us consider a two-dimensional metallic cylinder in a free space as shown in Fig. 1, the cylinder is parallel to z axis, while the cross-section of the cylinder is arbitrary. The object is illuminated by Gaussian pulse line source located at the points denoted by Tx and reflected waves are recorded at those points denoted by Rx. The computational domain is discretized by Yee cells [24]. It should be mentioned that the computational domain is surrounded by the optimized perfect matching layers (PML) absorber [25] to reduce the reflection from the environment-PML interface.

For the forward scattering problem the shape and location of the perfectly conducting cylinder to be determined is given first, and then the FDTD code with coarse grids is employed to calculate the scattered E fields that are utilized to mimic the experiments. It should be noted that in the forward problem, the shape function $F(\theta)$ of the 2-D perfectly conducting cylinder is described by the trigonometric series in this study as follows:

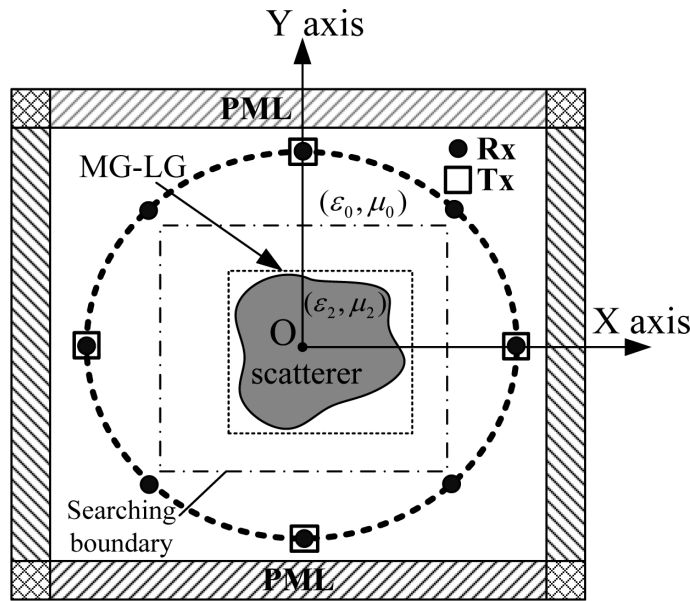$$F(\theta) = \sum_{n=0}^{N/2} B_n \cos(n\theta) + \sum_{n=1}^{N/2} C_n \sin(n\theta) \tag{1}$$

Fig. 1. Geometry for the inverse scattering of a perfectly conducting cylinder of arbitrary shape in free space.
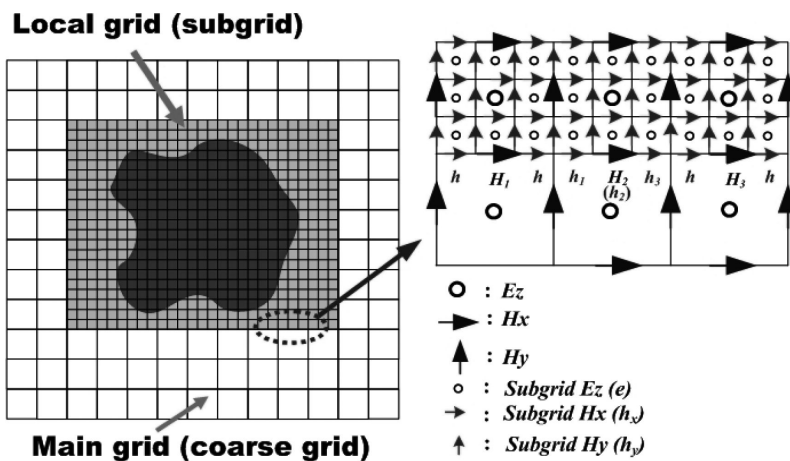

Fig. 2. The structure of the TM$_z$ FDTD major grids and local grids for the scaling ratio (1:3), H fields are aligned with the MG-LG boundary.

In order to closely describe the shape of the cylinder for both the forward and inverse scattering procedures, the subgridding technique is implemented in the FDTD code; the details are presented next.

In Fig. 2, E and H stand for the electric and magnetic fields on the major grids, respectively, while e and h denote the electric and magnetic fields on the local grids. If the scaling ratio is set at odd-ratio, for example $1:3$, the E and H fields coincide with e and h fields in the fine region as shown in Fig. 2. Note that the e and fields inside the fine region can be updated through the normal Yee-cell algorithm except those at the MG-LG boundary, such as h_1, h_2 and h_3 in Fig. 2.

The h fields at the MG-LG interface can be linearly interpolated as follows:

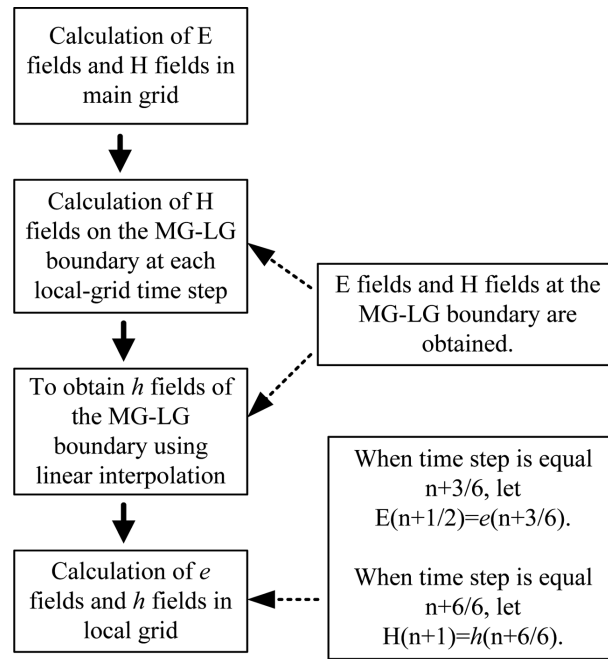$$h_1^{n+v} = H_1^{n+v} + \frac{2}{3}\left(H_2^{n+v} - H_1^{n+v}\right)$$

```
┌─────────────────────┐
│ Calculation of E     │
│ fields and H fields in│
│ main grid            │
└─────────────────────┘
          ↓
┌─────────────────────┐          ┌─────────────────────┐
│ Calculation of H     │ ◁┄┄┄┄┄  │ E fields and H fields at the│
│ fields on the MG-LG  │          │ MG-LG boundary are  │
│ boundary at each     │          │ obtained.           │
│ local-grid time step │          └─────────────────────┘
└─────────────────────┘
          ↓
┌─────────────────────┐          ┌─────────────────────┐
│ To obtain h fields of│          │ When time step is equal│
│ the MG-LG            │          │ n+3/6, let          │
│ boundary using       │          │ E(n+1/2)=e(n+3/6).  │
│ linear interpolation │          │                     │
└─────────────────────┘          │ When time step is equal│
          ↓                       │ n+6/6, let          │
┌─────────────────────┐          │ H(n+1)=h(n+6/6).    │
│ Calculation of e     │ ◁┄┄┄┄┄  └─────────────────────┘
│ fields and h fields in│
│ local grid           │
└─────────────────────┘
```

Fig. 3. The flowchart to update the (E,H) fields on the major grids and (e, h) fields on local grids.

$$h_2^{n+v} = H_2^{n+v}, \quad \text{for} v = \frac{1}{3}, \frac{2}{3} \text{and} \frac{3}{3}.$$
$$h_3^{n+v} = H_2^{n+v} + \frac{1}{3}\left(H_3^{n+v} - H_2^{n+v}\right) \qquad (2)$$

Note that the H fields don't exist on the main grids actually for $v = \frac{1}{3}$ and $\frac{2}{3}$ and need extra parabolic interpolation calculation by

$$H^{n+v} = H^n + Av + \frac{Bv^2}{2} \qquad (3)$$

with $A = \frac{H^{n+1} - H^{n-1}}{2}$

$$B = H^{n+1} - H^{n-1} - 2H^n$$

The corresponding flow chart for updating the EM fields in the fine region is shown in Fig. 3. Note that at the time step the fields on the main grids should be updated by the coincided fields on the local grids. Similarly, at the time step $n + \frac{6}{6}$ the H^{n+1} fields are updated by the coincided $h^{n+\frac{6}{6}}$ fields.

For the time domain scattering and/or inverse scattering problem, the scatterers are assigned with the fine region such that the fine structure can be easily described. If higher resolution is needed, only the fine region needs to be rescaled using a higher ratio for subgridding. This can avoid gridding the whole problem space using the finest resolution such that the computational resources are utilized in a more efficient way, which is quite important for the computationally intensive inverse scattering problems. More detail on the FDTD-Subgridding scheme can be found in [22]

For the time domain scattering and/or inverse scattering problem, the scatterers can be assigned with the fine region such that the fine structure can be easily described. If higher resolution is needed, only

the fine region needs to be rescaled using a higher ratio for subgridding. This can avoid gridding the whole problem space using the finest resolution such that the computational resources are utilized in a more efficient way, which is quite important for the computational intensive inverse scattering problems.

3. Inverse problem

The first set of E field data is obtained in the forward problem by the FDTD code with fine grids to mimic the experiment measurement data, while the second set of E field data is obtained in the inverse problem by the FDTD code with coarse grids. The second E field data are obtained in the inverse problem by the FDTD code with coarse grids. As compared with the first E field data obtained in the forward scattering procedure, the inverse scattering problem can be formulated into an optimization problem. The proposed global searching APSO and PSO scheme are employed to reconstruct the location, shape and permittivity of the perfectly conducting cylinder under test by minimizing the errors between two E filed dates.

During the course of optimization process, the following objective function (*OF*) is defined for each candidate cylinder in the APSO scheme:

$$OF = \frac{\sum\limits_{n=1}^{N_i} \sum\limits_{m=1}^{M} \sum\limits_{b=0}^{B} \left| E_z^{exp}(n, m, b\Delta t) - E_z^{cal}(n, m, b\Delta t) \right|}{\sum\limits_{n=1}^{N_i} \sum\limits_{m=1}^{M} \sum\limits_{b=0}^{B} \left| E_z^{exp}(n, m, b\Delta t) \right|} \tag{4}$$

Where E_z^{exp} and E_z^{cal} are experimental electric fields and the calculated electric fields, respectively. The N_i and M are the total number of the transmitters and receivers, respectively. B is the total time step number of the recorded electric fields. The details of the proposed PSO and APSO are represented as follows.

3.1. Modified asynchronous Particle swarm optimization (APSO)

Particle swarm global optimization is a class of derivative-free, population-based and self-adaptive search optimization technique. Particles (potential solutions) are distributed throughout the searching space and their positions and velocities are modified based on social behavior. The social behavior in PSO is a population of particles moving towards the most promising region of the search space. Clerc [31] proposed the constriction factor to adjust the velocity of the particle for obtaining the better convergence; the algorithm was named as constriction factor method. PSO starts with an initial population of potential solutions that is randomly generated and composed N_p individuals (also called particles). Each individual contains certain number of the shape parameters (eleven unknown parameters in our test cases), which includes the center position, the radius and the slope of the cubic spline to describe the cylinder shape.

After the initialization step, each particle of population has assigned a randomized velocity and position. Thus, each particle has a position and velocity vector, and moves through the problem space. In each generation, the particle changes its velocity by its best experience, called x_{pbest}, and that of the best particle in the swarm, called x_{gbest}.

Assume there are N_p particles in the swarm that is in a search space in D dimensions, the position and velocity could be determine according to the following equations (constriction factor method):

$$v_{id}^k = \chi \cdot \left(v_{id}^{k-1} + c_1 \cdot \varphi_1 \cdot \left(x_{pbest,\ id} - x_{id}^{k-1} \right) + c_2 \cdot \varphi_2 \cdot \left(x_{gbest,\ id} - x_{id}^{k-1} \right) \right) \tag{5}$$

$$x_{id}^k = x_{id}^{k-1} + v_{id}^k \tag{6}$$

where $\chi = \dfrac{2}{\left|2-\phi-\sqrt{\phi^2-4\phi}\right|}$, $\phi = c_1 + c_2 \geqslant 4$. c_1 and c_2 are learning coefficients, used to control the impact of the local and global component in velocity Eq. (3). v_{id}^k and x_{id}^k are the velocity and position of the i-th particle in the d-th dimension at k-th generation, φ_1 and φ_2 are both the random number between 0 and 1. The "damping boundary condition" proposed by Huang and Mohan [32] to ensure the particles move within the legal search space.

The key distinction between APSO and a typical synchronous PSO is on the population updating mechanism. In the synchronous PSO, the algorithm updates all the particles velocities and positions using Eqs (3) and (4) at end of the generation. And then update the best positions, x_{pbest} and x_{gbest}. Alternatively, the updating mechanism of APSO is that the new best position is found after each particle position updates if the new position is better than the current best position. The new best position will be used in following particles swarm immediately. The swarm reacts more quickly to speedup the convergence because the updating occurs immediately after objective function evaluation for each particle.

The flowchart of the APSO is shown in Fig. 4. APSO goes through seven procedures as follows:

   I. Initialize a starting population: Randomly generate a swarm of particles that consists of the shape parameters.
  II. Calculate E fields by a home-made FDTD code.
 III. Evaluate the population using objective function: The APSO algorithm evaluates the objective function Eq. (4) for each individual in the population.
  IV. Find x_{pbest} and x_{gbest}.
   V. Mutation scheme: The PSO algorithm has been shown to converge rapidly during the initial stages of a global search, but when around global optimum, the search can become very slow. For the reason, mutation scheme is introduced in this algorithm to speed up the convergence when particles are around global optimum. The mutation scheme can also avoid premature convergences in searching procedure and help the x_{gbest} escape from the local optimal position. As shown in Fig. 4, there is an additional competition between the x_{gbest} and $x_{pbest_{mu}}$. The current x_{gbest} will be replaced by the $x_{gbest\ mu}$ if the $x_{gbest\ mu}$ is better than the current x_{gbest}. The $x_{gbest\ mu}$ is generated by following way:

$$X_{gbest_{mu}} = \begin{cases} X_{gbest} - \varphi_3 \cdot \left[c_3 - (c_3 - c_4) \cdot \frac{k}{k_{\max}}\right] \cdot (x_{\max} - x_{\min}), \; if \; \varphi_{mu} < 0.5 \\ X_{gbest} + \varphi_3 \cdot \left[c_3 - (c_3 - c_4) \cdot \frac{k}{k_{\max}}\right] \cdot (x_{\max} - x_{\min}), \; if \; \varphi_{mu} \geqslant 0.5 \end{cases} \tag{7}$$

where c_3 and c_4 are the scaling parameter. φ_3 and φ_{mu} are both the random number between 0 and 1. k is the current iteration number. $k_{\max}$ is the maximum iteration number. $x_{\max}$ and $x_{\min}$ are the upper limit and lower limit of the search space, respectively.
  VI. Update the velocity and position.
 VII. Stop the process and print the best individual if the termination criterion is satisfied, else go to step II.

3.2. Cubic spline interpolation technique

It should be noted that in the inverse problem, the shape function of the 2-D metallic cylinder is described by a cubic spline in this study instead of the trigonometric series described in the section of
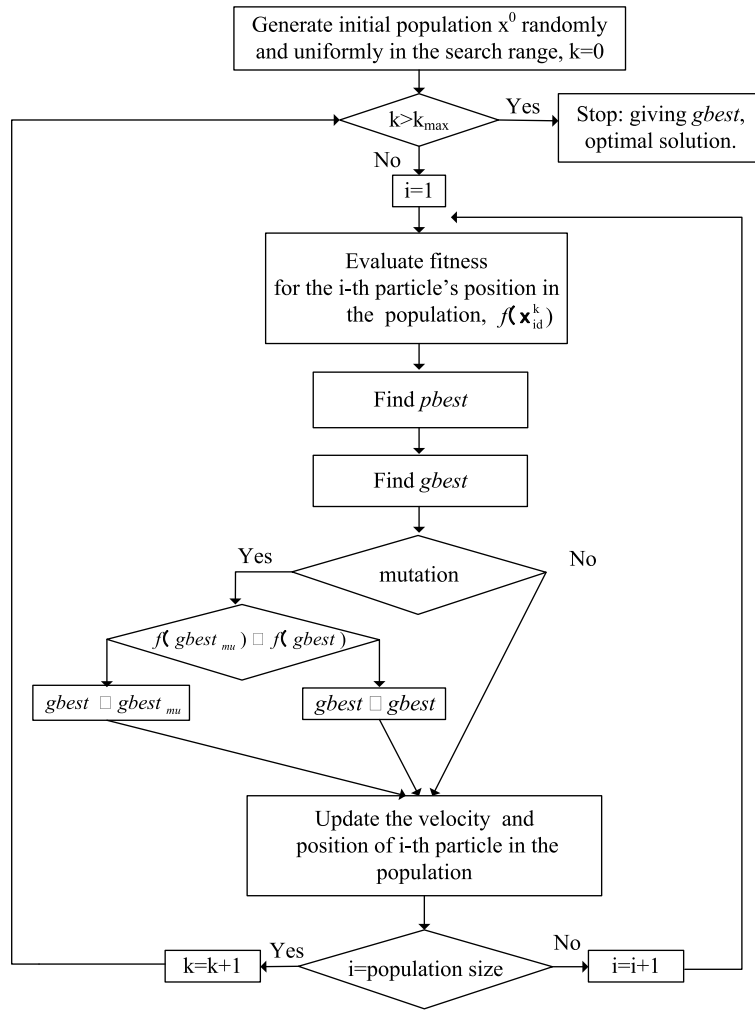
Fig. 4. Flowchart for the asynchronous particle swarm optimization.

the forward problem. The cubic spline is more efficient in terms of the unknown number required to describe a cylinder of arbitrary cross section. By using the cubic spline the coordinates of local origin inside the cylinder serve as the searching parameter and can move around the searching space, which is impossible if the trigonometric series expansion is used in the inversion procedure.

As shown in Fig. 5, the cubic spline consists of the polynomials of degree 3 $P_i(\theta)$, $i = 1, 2, \cdots, N$, which satisfy the following smooth conditions:

$$P_i(\theta_i) = P_{i+1}(\theta_i) \equiv \rho_i$$

$$P_i'(\theta_i) = P_{i+1}'(\theta_i) \quad i = 1, 2, \cdots, N \tag{8}$$

$$P_i''(\theta_i) = P_{i+1}''(\theta_i)$$

and
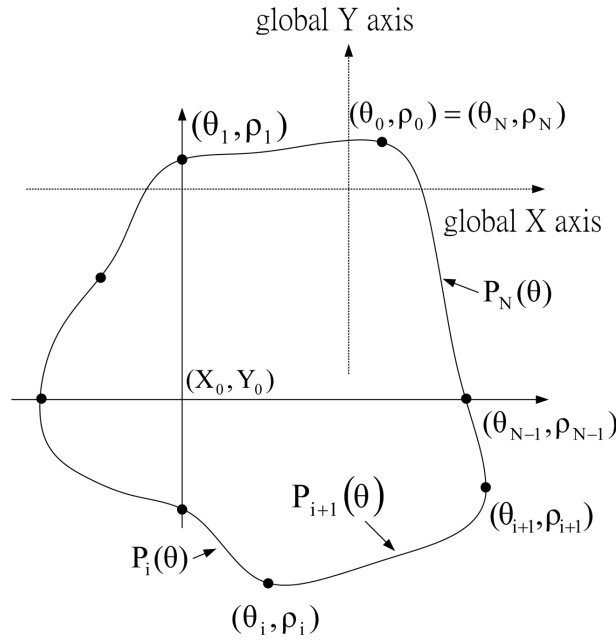
$$P_1(\theta_0) = P_N(\theta_N)$$

Fig. 5. A cylinder of arbitrary shape is described in terms of a closed cubic spline.

$$P_1'(\theta_0) = P_N'(\theta_N) \equiv \rho_N' \tag{9}$$

$$P_1''(\theta_0) = P_N''(\theta_N)$$

Through the interpolation of the cubic spline, an arbitrary smooth cylinder can be easily described through the radius parameters $\rho_1, \rho_2, \cdots, \rho_N$ and the slope ρ_N', of which the details are referred to [23]. By combining the modified APSO and the cubic spline interpolation technique, we are able to reconstruct the microwave image efficiently.

It should be noted that the coordinates of local origin inside the cylinder plus the radiuses of the geometrical spline used to describe the shape of the cylinder will be determined by the APSO and PSO scheme.

4. Numerical results

As shown in Fig. 1, the problem space is divided in 68×68 grids with the grid size $\Delta x = \Delta y = 5.95$ mm. The metallic cylinder is located in free space. The cylindrical object is illuminated by a transmitter at four different positions, $N_i = 4$. The scattered E fields for each illumination are collected at the eight receivers, $M = 8$. Note that the simulated result using one incident wave is much worse than that by two incident waves. In order to get accurate result, four transmitters are used here. The transmitters and receivers are collocated at a distance of 24 grids from the origin. The incident current pulse $I_z(t)$ is expressed as:

$$I_z(t) = \begin{cases} Ae^{-\alpha(t-\beta\Delta t)^2} & , t \leq T_w \\ 0 & , t > T_w \end{cases} \tag{10}$$
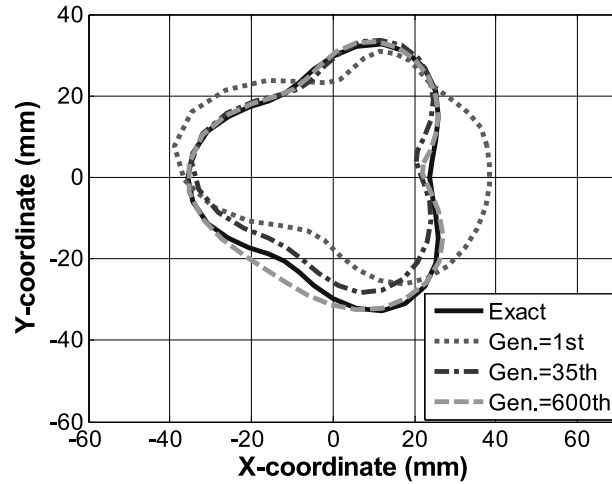
Fig. 6. The reconstructed shape of the cylinder at different generations for example 1 by APSO.

where $\beta = 24$, $A = 1000$, $\Delta t = 13.337ps$, $T_w = 2\beta\Delta t$, and $\alpha = \left(\frac{1}{4\beta\Delta t}\right)^2$.

The time duration is set to $250 \Delta t(T = 250)$. Note that in order to accurately describe the shape of the cylinder, the subgridding FDTD technique is used both in the forward scattering (1:9) and the inverse scattering (1:5) parts – but with different scaling ratios as indicated in the parentheses. For the forward scattering, the E fields generated by the FDTD with fine subgrids are used to mimic the experimental data in Eq. (4).

Two examples are investigated for the inverse scattering of the proposed structure by using the modified APSO. There are eleven unknown parameters to retrieve, which include the center position (X_O, Y_O), the radius $\rho_i, i = 1, 2, \cdots, 8$ of the shape function and the slope ρ'_N. Very wide searching ranges are used for the modified APSO to optimize the objective function given by Eq. (7). The parameters and the corresponding searching ranges are listed follows: -47.6 mm $\leqslant X_O \leqslant$ 47.6 mm, -47.6 mm $\leqslant Y_O \leqslant$ 47.6 mm, 5.95 mm $\leqslant \rho_i \leqslant$ 71.4 mm, $i = 1,2, \cdots, 8, -1 \leqslant \rho'_N \leqslant 1$. The operational coefficients for the PSO are set out below. The learning coefficients, c_1 and c_2, are set to 2 [33], and the population size is set to 30. The relative coefficient of the modified APSO are set as below: The learning coefficients, c_1 and c_2, are set to 2.8 and 1.3 respectively. The mutation probability is 0.1 and the population size is set to 30 [34].

For the first example, the metallic cylinder with shape function $F(\theta) = 29.75 - 5.95\cos(3\theta)$ mm is considered. The final reconstructed shape by APSO at the 600th generation is compared to the exact shape in Fig. 6. The final reconstructed shapes by PSO and APSO at the 600th generation are compared to the exact shape in Fig. 7. The discrepancy of shape Function (DF) of the reconstructed shape $F^{cal}(\theta)$ with respect to the exact values versus generations is shown in Fig. 8. It is shown that the APSO scheme is able to achieve good convergences within 50 generations. Here, DF is defined as

$$DF = \{\frac{1}{N'} \sum_{i=1}^{N'} [F^{cal}(\theta_i) - F(\theta_i)]^2 / F^2(\theta_i)\}^{1/2} \tag{11}$$

where the N' is set to 720. The r.m.s. error DF for PSO and APSO are about 17.3% and 5.32% in the final generation, respectively. In order to investigate the sensitivity of the imaging algorithm against
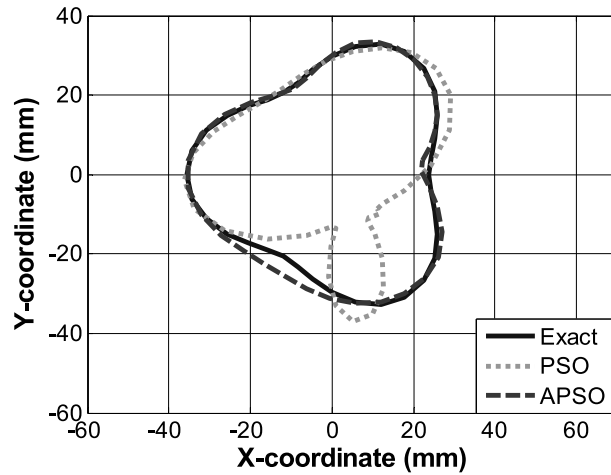
Fig. 7. The reconstructed shapes of the cylinder for example 1 by PSO and APSO, respectively.
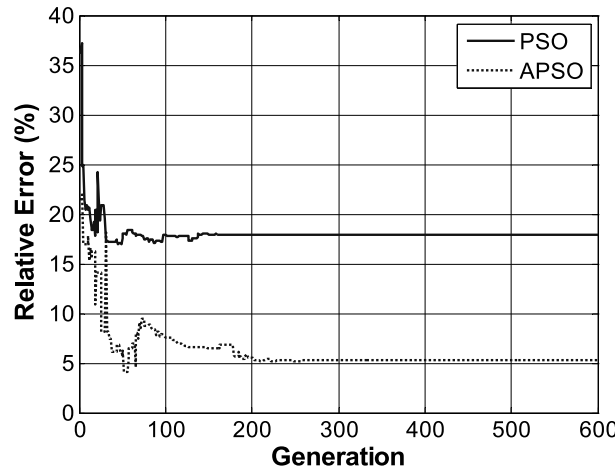

Fig. 8. Shape function error versus generation for example 1 by PSO and APSO, respectively.

random noise, the additive white Gaussian noise of zero mean with standard deviation σ_g is added into the scattered electric fields to mimic the possible measurement errors. The relative noise level (RNL) is defined as:

$$RNL = \frac{\sigma_g}{\sqrt{\dfrac{\sum\limits_{n=1}^{Ni}\sum\limits_{m=1}^{M}\sum\limits_{k=0}^{K}\left|E_z^{\exp}(n,m,k\Delta t)\right|^2}{(N_i)(M_i)(K+1)}}} \tag{12}$$

The relative noise level of 10^{-4}, 10^{-3}, 10^{-2} and 0.1 are used in PSO and APSO for simulation purpose. Figure 9 shows the reconstructed results under the condition that the experimental scattered field is contaminated by the noise. It could be observed that good reconstruction has been obtained for shape of the metallic cylinder when the relative noise level is below 10^{-1}.

In the second example, we would like to test the robustness of the algorithm for the complex shapes, the metallic cylinder with shape function $F(\theta) = 29.75 + 5.95\cos(4\theta)$ mm is considered. The final
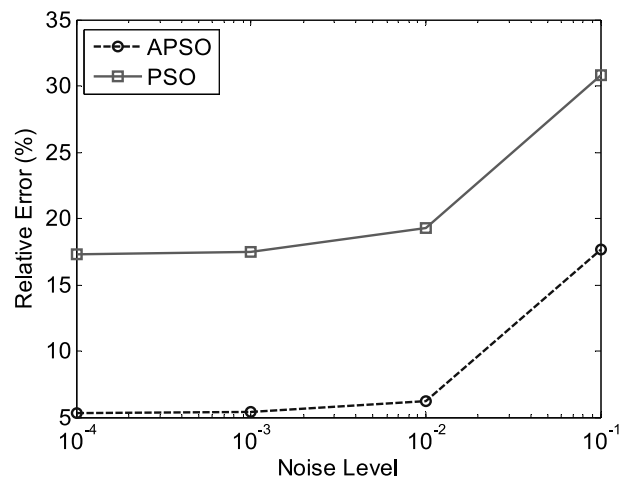
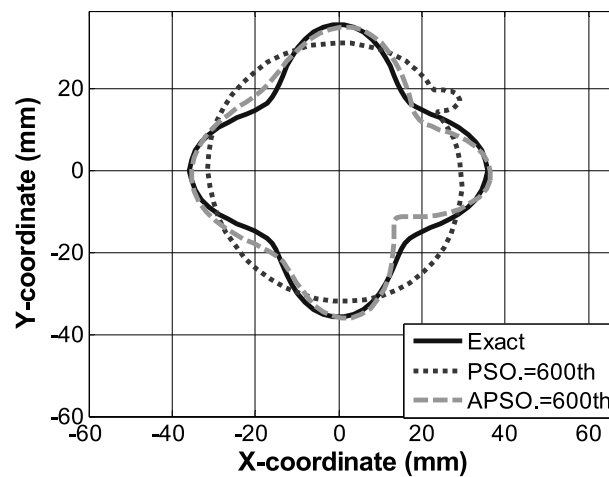Fig. 9. Shape error as function of RNL by PSO and APSO, respectively.

Fig. 10. The reconstructed shapes of the cylinder for example 2 by PSO and APSO, respectively.

reconstructed shapes by PSO and APSO at the 600th generation are compared to the exact shape in Fig. 10. Figure 11 shows that APSO the relative errors of the shape decrease quickly and good convergences are achieved within 40 generation. The r.m.s. error DF for PSO and APSO are about 17.9% and 8.55% in the final generation, respectively. From the reconstructed results this object, we conclude the APSO scheme can be used to reconstruct metallic cylinder. For complex shapes, it is found that APSO has better reconstruction results than PSO does.

5. Conclusion

In this paper, we study the time domain inverse scattering of an arbitrary cross section metallic cylinder in free space. By combining the FDTD method and the APSO, good reconstructed results are obtained. The key differences between PSO [16] and APSO are about the convergence speed, the computation time
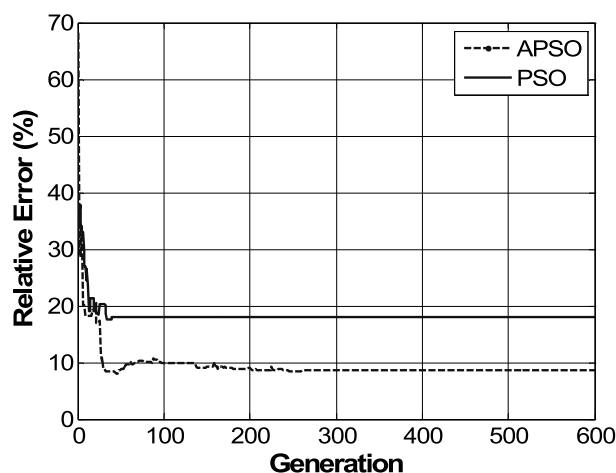
Fig. 11. Shape function error versus generation for example 2 by PSO and APSO, respectively.

and the accuracy, since APSO includes "damping boundary condition" scheme and mutation scheme. The subgridding scheme is employed to closely describe the shape of the cylinder for the FDTD method. Some stabilization techniques to avoid the mismatch at the MG-LG interface are adopted. In order to describe the shape of the scatterer more effectively, cubic spline interpolation technique is utilized. The inverse problem is reformulated into an optimization one, and then the global searching scheme APSO is employed to search the parameter space. By using the APSO, the shape of the object can be successfully reconstructed. In our study, even when the initial guess is far from the exact one, the APSO can still yield a good solution for the properties of the object. Numerical results have been carried out and good reconstruction has been obtained even in the presence of white Gaussian noise in experimental data.

References

[1]   J. Ch. Bolomey, D. Lesselier, C. Pichot and W. Tabbara, Spectral and time domain approaches to some inverse scattering problems, *IEEE Transactions on Antennas and Propagation* **AP-29** (1981), 206–212.
[2]   S. Coen, K.K. Mei and D.J. Anelakos, Inverse scattering technique applies to remote sensing of layered media, *IEEE Transactions on Antennas and Propagation* **29** (1981), 298–306.
[3]   W. Chien, C.H. Sun and C.C. Chiu, Image Reconstruction for a Partially Immersed Imperfectly Conducting Cylinder by Genetic Algorithm, *International Journal of Imaging Systems and Technology* **19** (Dec 2009), 299-305.
[4]   C.H. Sun, C.L. Liu, K.C. Chen, C.C. Chiu, C.L. Li and C.C. Tasi, Electromagnetic Transverse Electric Wave Inverse Scattering of a Partially Immersed Conductor by Steady-State Genetic Algorithm, *Electromagnetics* **28**(6) (Aug 2008), 389–400.
[5]   C.H. Huang, Y.F. Chen and C.C. Chiu, Permittivity Distribution Reconstruction of Dielectric Objects by a Cascaded Method, *Journal of Electromagnetic Waves and Applications* **21**(2) (Jan 2007), 145–159.
[6]   E. Abenius and B. Strand, Solving inverse electromagnetic problems using FDTD and gradient-based minimization, *International Journal for Numerical Methods in Engineering* **68**(6) (Nov 2006), 650–673.
[7]   X. Chen, D. Liang and K. Huang, Microwave Imaging 3-D Buried Objects Using Parallel Genetic Algorithm Combined With FDTD Technique, *Journal of Electromagnetic Waves and Applications* **20**(13) (2006), 1761–1774.
[8]   I.T. Rekanos, Time-domain inverse scattering using lagrange multipliers: an iterative FDTD-based optimization technique, *Journal of Electromagnetic Waves and Applications* **17**(2) (2003), 271–289.
[9]   D. Colton and R. Kress, *Inverse Acoustic and Electromagnetic Scattering Theory*, New York: Springer-Verlag, 1992.
[10] M. Benedetti, M. Donelli and A. Massa, Multicrack Detection in Two-Dimensional Structures by Means of GA-Based Strategies, *IEEE Transaction on Antennas and Propagation* **55**(1) (Jan 2007), 205–215.

[11] C.L. Li, W. Chien, C.H. Huang and C.C. Chiu, Time Domain Microwave Imaging for a Buried Dielectric Cylinder by Dynamic Differential Evolution, *International Journal of Applied Electromagnetics and Mechanics* **34**(1, 2) (Nov 2010), 73–86.

[12] R.A. Wildman and D.S. Weile, Greedy Search And A Hybrid Local Optimization/Genetic Algorithm For Tree-Based Inverse Scattering, *Microwave and Optical Technology Letters* **50**(3) (Mar 2008), 822–825.

[13] C.H. Sun, C.C. Chiu, C.L. Li and C.H. Huang, Time Domain Image Reconstruction for Homogenous Dielectric Objects by Dynamic Differential Evolution, *Electromagnetics* **30**(4) (May 2010), 309–323.

[14] W. Chien, C.H. Huang, C.C. Chiu and C.L. Li, Image Reconstruction for 2D Homogeneous Dielectric Cylinder Using FDTD Method and SSGA, *International Journal of Applied Electromagnetics and Mechanics* **32**(2) (Feb 2010), 111–123.

[15] I.T. Rekanos, Shape Reconstruction of a Perfectly Conducting Scatterer Using Differential Evolution and Particle Swarm Optimization, *IEEE Transactions on Geoscience and Remote Sensing* **46**(7) (Jul 2008), 1967–1974.

[16] C.H. Huang, C.C. Chiu, C.L. Li and K.C. Chen, Time Domain Inverse Scattering of a Two-Dimensional Homogenous Dielectric Object with Arbitrary Shape by Particle Swarm Optimization, *Progress In Electromagnetic Research* **PIER 82** (February 2008), 381–400.

[17] M. Donelli and A. Massa, Computational approach based on a particle swarm optimizer for microwave imaging of two-dimensional dielectric scatterers, *IEEE Trans Microw Theory Tech* **53**(5) (May 2005), 761–1776.

[18] M. Donelli, G. Franceschini, A. Martini and A. Massa, An integrated multiscaling strategy based on a particle swarm algorithm for inverse scattering problems, *IEEE Trans Geosci Remote Sens* **44**(2) (Feb 2006), 298–312.

[19] W. Chien and C.C. Chiu, Using NU-SSGA to Reduce the Searching Time in Inverse Problem of a Buried Metallic Object, *IEEE Transactions on Antennas and Propagation* **53**(10) (Oct 2005), 3128–3134.

[20] A. Semnani, M. Kamyab and I.T. Rekanos, Reconstruction of One-Dimensional Dielectric Scatterers Using Differential Evolution and Particle Swarm Optimization, *IEEE Geoscience and Remote Sensing Letters* **6**(4) (Oct 2009), 671–675.

[21] I.T. Rekanos, Shape Reconstruction of a Perfectly Conducting Scatterer Using Differential Evolution and Particle Swarm Optimization, *IEEE Transactions on Geoscience and Remote Sensing* **46**(7) (Jul 2008), 1967–1974.

[22] M.W. Chevalier, R.J. Luebbers and V.P. Cable, FDTD local grid with material traverse, *IEEE Trans Antennas and Propagation* **45**(3) (March 1997).

[23] C. de Boor, *A Practical Guide to Splines*, Springer-Verlag, New York, 1978.

[24] K. Yee, Numerical solutions of initial boundary value problems involving Maxwell's equations in isotropic media, *IEEE Transactions on Antennas and Propagation* **AP-14** (1966), 302–307.

[25] C.L. Li, C.W. Liu and S.H. Chen, Optimization of a PML Absorber's Conductivity Profile using FDTD, *Microwave and Optical Technology Letters* **37** (2003), 380–383.

[26] Y. Zhou, J. Li and H. Ling, Shape inversion of metallic cavities using hybrid genetic algorithm combined with tabu list, *Electronics Letters* **39** (Feb 2003), 280–281.

[27] W. Chien and C.C. Chiu, Cubic-Spline Expansion with GA for Half-Space Inverse Problems, *Applied Computational Electromagnetics Society Journal* **20**(2) (July 2005), 136–143.

[28] W. Chien and C.C. Chiu, Cubic-Spline expansion with GA for a Partially Immersed Conducting Cylinder, *IEICE Trans Electron* **E88-C**(12) (Dec 2005), 2223–2228.

[29] W. Chien, C.C. Chiu and C.L. Li, Cubic-Spline Expansion with GA for a Conducting Cylinder Buried in a Slab Medium, *Electromagnetics* **26**(5) (July 2006), 329–343.

[30] W. Chien, C.H. Huang and C.C Chiu, Cubic-Spline expansion for a Two-Dimensional Periodic Conductor in Free Space, *International Journal of Applied Electromagnetics and Mechanics* **24**(1–2) (Nov 2006).

[31] M. Clerc, The swarm and the queen: towards a deterministic and adaptive particle swarm optimization, *Proceedings of Congress on Evolutionary Computation*, Washington, DC, 1951–1957, 1999.

[32] T. Huang and A.S. Mohan, Application of particle swarm optimization for microwave imaging of lossy dielectric objects, *IEEE Antenna and Propagation Society International Symposium Digest* (2005), 852–855.

[33] J. Kennedy and R. Eberhart, Particle Swarm Optimization, *Proceedings of the 1995 IEEE International Conference on Neural Networks*, 1942–1948.

[34] A. Carlisle and G. Dozier, An Off-The-Shelf PSO, *Proceedings of the 2001 Workshop on Particle Swarm Optimization* (2001), 1–6.